Laser Radar in Ballistic Missile Defense

Isaac N. Bankman, Eric W. Rogala, and Richard E. Pavek

Against many ballistic missile types, radar and passive infrared sensors can identify the warhead and guide the interceptor to an effective impact. However, new ballistic missiles that deploy countermeasures such as decoys, jammers, chaff, and flares pose a significant challenge for these two sensors. One possible solution is to introduce laser radar (ladar) among the sensors for Ballistic Missile Defense. This article presents the physical advantages and limitations of ladar, its potential role as part of a seeker, the data it can provide, and techniques for identifying the warhead.

INTRODUCTION

Although Navy and Army programs have demonstrated that unitary ballistic missiles can be intercepted with current technology, separating ballistic missiles remain some of the most lethal yet elusive targets in air defense. The threat they pose has prompted numerous studies and development projects ranging from detector physics to end-to-end interception simulations. Separating ballistic missiles can deploy several types of objects in flight. The warhead, known as the reentry vehicle (RV) when the trajectory is exo-atmospheric, may be accompanied by the attitude control module and booster segments as well as countermeasures such as balloons, lightweight decoys, jammers, and chaff. The high speed and spatial spread of these objects require a seeker that can sense and identify the warhead from long distances to allow enough time for interceptor dynamics and terminal guidance. Yet the small size of the objects and the presence of countermeasures create a considerable challenge for current sensors at distances of interest. Radar and passive infrared (IR) jointly serve well for intercepting unitary targets and some separating missiles, but their capability may need to be complemented by another type of sensor to cope with many other separating ballistic missiles with countermeasures.

Sensor Functions

Long-range ballistic missile trajectories reach very high altitudes, and the RV travels a significant fraction of the time in the exo-atmosphere. In such cases, the RV is typically spin-stabilized to ensure that it does not deviate from its intended ballistic trajectory. Therefore, identification of the spinning RV is particularly important, and sensors and algorithms should address the specific signatures presented by the spinning RV. In some ballistic missiles the RV is not spin-stabilized, and it tumbles along its trajectory. During engagement, once the RV is discriminated from all other objects, the seeker on the interceptor must determine the aimpoint on the RV for terminal guidance and effective impact. Laser radar (ladar) in Ballistic Missile Defense can contribute to three essential functions of the seeker:

(1) discrimination of the spinning RV, (2) discrimination of the tumbling RV, and (3) aimpoint selection.

To discriminate the RV, all candidate objects must be observed, and discrimination algorithms must compare measurements from all observed objects. Discrimination must start early enough in the engagement so that, by the time it is completed, the distance remaining between interceptor and RV allows the interceptor to divert to the RV and home in on the selected aimpoint. Therefore, if closing speeds are high, discrimination has to be completed at distances greater than 200 km from the target, whereas in engagements with low closing speeds, it may be possible to defer discrimination to shorter distances. At distances required for discrimination, each object appears as one pixel in passive IR images, and discrimination is possible if the RV can be distinguished by its intensity or variation of intensity across time. Radar also can contribute to discrimination with information that relates to the object's length and motion. Aimpoint selection requires significantly high angular resolution, which may be difficult to achieve with current radars. Passive IR can provide a sufficiently resolved image of the RV for aimpoint selection when the distance is shorter than 20 km.

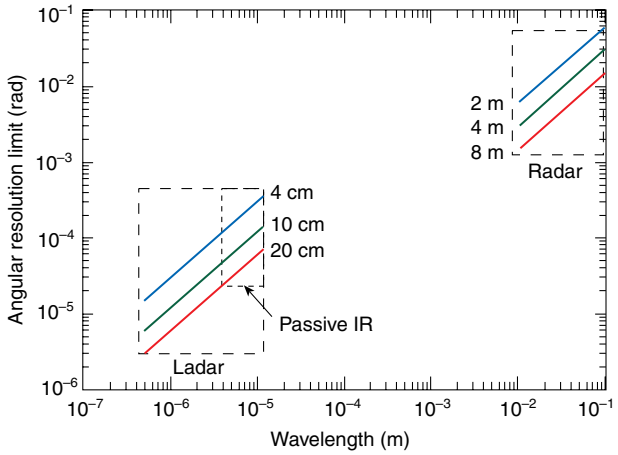

Figure 1. Fundamental angular resolution limit due to diffraction at wavelengths of radar, passive IR, and ladar for varying aperture diameters.

Ladar Compared to Radar and Passive IR

To complement radar in observing ballistic missiles, the additional sensor must have higher resolution in angle or Doppler measurements or must be insensitive to radio-frequency (RF) countermeasures. To complement passive IR in ballistic missile applications, the additional sensor must provide range or Doppler measurements, have higher angular resolution, or be insensitive to IR countermeasures. Furthermore, it should be able to infer information on the shape, orientation, and motion of the objects. Owing to its shorter wavelengths, ladar is a good candidate to meet these requirements, within the confines of its own limits imposed by physics, technology, and tactical setting. The shortest radar wavelengths in ballistic missile applications are around 1 cm, and the passive IR signal is typically between 4 and 12 μm. Ladar wavelengths can be as low as 0.5 μm, and devices that produce shorter wavelengths are under development. Shorter wavelengths provide higher resolution in angular and Doppler measurements.

The fundamental physical angular resolution limit of a sensor operating at a wavelength λ and with aperture diameter d is $1.22\lambda/d$. Examples of angular resolution limits are shown in Fig. 1 for the three types of sensors with varying apertures. Although radar antennas can be 2 orders of magnitude larger than ladar telescopes, the angular resolution of ladar can be 3 orders of magnitude finer than that of radar. For a given aperture, and at the same distance from the target, a ladar system operating at 1 μm has 4 times better angular resolution than a passive IR system operating at 4 μm. With the same aperture, ladar can provide the appropriate spatial cross-range resolution, such as 10 to 20 cm, from a distance 4 times longer compared to passive IR. This extended sensing distance results in more available time for guidance corrections. Figure 2 illustrates the expected differences between ladar and passive IR images obtained with an aperture of 20 cm at varying distances to the target. For both sensors, the magnification in Fig. 2 was adjusted in the simulation to provide the same field of view at all distances, and the quantization by the detector array was not introduced. This allows simulation of the optical information at the aperture and effective comparison of the physical resolution differences due to diffraction only.

Absolute frequency resolution, the smallest observable step in frequency, is the inverse of observation time and does not depend on wavelength. However, the relative frequency quantization introduced with a given absolute frequency resolution depends on the Doppler extent of a received signal, which in turn is inversely proportional to wavelength. Consequently, for a given observation time, a ladar operating with a 10-μm wavelength provides 3000 times finer frequency quantization than a 10-GHz radar where the wavelength is 3 cm. Alternatively, informative frequency quantizations in ladar at 10 and 1 μm can be obtained with observation times that are 3 to 4 orders of magnitude shorter compared to radar. Fast observations can be a significant advantage, especially in applications such as Ballistic Missile Defense, where available time for sensing each object is severely limited.

Both radar and ladar can provide 10- to 20-cm range resolution, which is appropriate for Ballistic Missile Defense. Advanced techniques can also provide finer resolution for both sensors. Therefore, ladar does not yield an advantage in range measurement.

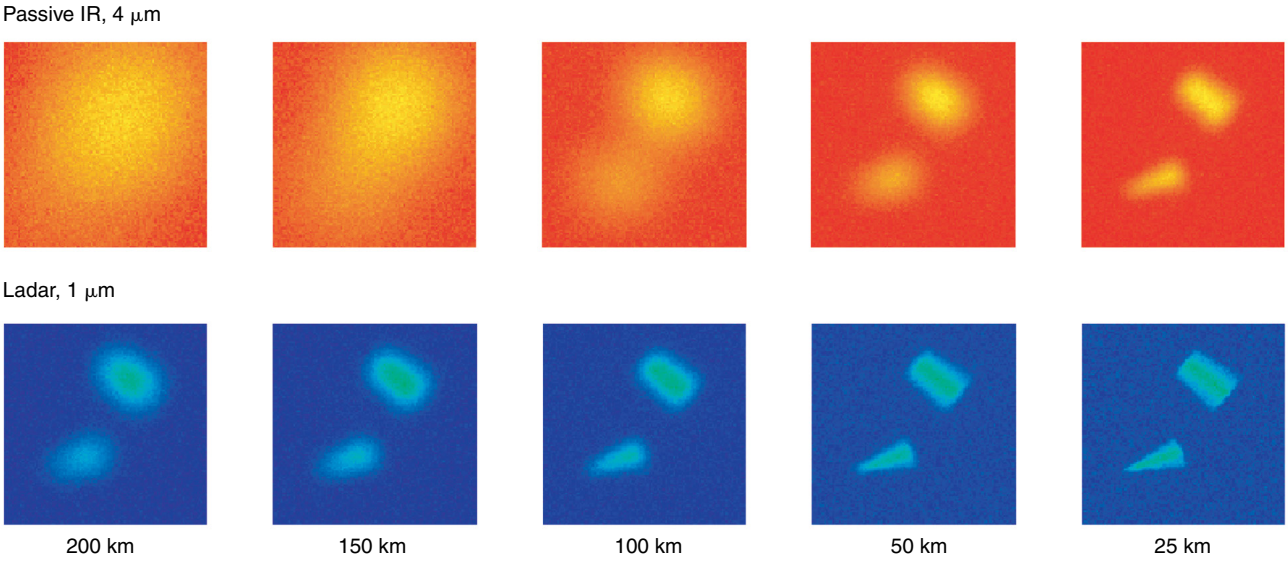

Figure 2. Comparison of physical resolution for 4 and 1 μm at five different distances from the target.

Chaff and other small objects that increase the noise background in radar have negligible impact on ladar sensing. Materials that reduce radar cross-section do not decrease the reflectance at ladar wavelengths to prohibitive levels. Jammers are designed for RF wavelengths and do not affect ladar detectors. Although ladar jammers may be conceived, they are not likely to be effective because the ladar field of view is typically less than 100 μrad. The precise location of the ladar and the orientation of its beam must be known to point a jammer and undermine ladar. Flares, which introduce spurious signals in the passive IR image, have a wide spectral content, and only a negligibly small level of flare emission is likely to be in the narrow ladar spectral band and ladar field of view. A jammer or a flare source would be observed by ladar only if the laser beam were pointed toward the object, in which case it would be discriminated from the RV because of its smaller size.

Limitations of Ladar

Shorter wavelengths that enable ladar's higher angular and spectral resolutions also introduce a fundamental physical disadvantage. Optical wavelengths are severely attenuated by the atmosphere and weather conditions such as fog and rain. Therefore, using a ladar located at sea level does not seem feasible for ballistic missile sensing where objects can be in the exoatmosphere. Ladar must operate from a high-altitude platform, preferably integrated in the interceptor missile itself, in a manner similar to passive IR. Other potential platforms for ladar are aircraft and satellites. The ladar transmitter power levels that can be achieved are limited by the size and weight allowed by the platform, as well as laser technology. Especially onboard a missile, ladar power levels will be limited and will confine feasible operational ranges. To maximize the power density within the illuminating beam, its divergence is typically kept at a very low angle. Because of its narrow beam operation, searching for ballistic missile targets is not practical with ladar, and either radar or passive IR must cue the ladar to point in the direction of potential targets and interrogate them.

Fundamental concepts related to wavelength, resolution, transmittance, and beamwidth suggest that ladar is well suited for synergistic operation with radar and passive IR. Nevertheless, the potential contribution of ladar to Ballistic Missile Defense remains to be determined. The added value of ladar depends on whether it will be capable of making some essential observations, measurements, or inferences significantly better than radar or passive IR.

Ladar Systems

As with radar, ladar[1–3] illuminates its target and observes the reflected wavefront (Fig. 3). The transmitter consists primarily of a laser cavity and optics for pulse modulation, beam shaping, and beam pointing. A telescope serves the same role as the antenna for radar. Ladar is mainly used in monostatic mode, i.e., when transmitter and receiver reside in the same location; however, bistatic mode is also possible. Here we will consider only the monostatic mode and assume that transmitter and receiver lines of sight overlap. The backscattered wavefront is collected by the telescope aperture and focused on the detector of the receiver. In incoherent detection, the detector simply produces an

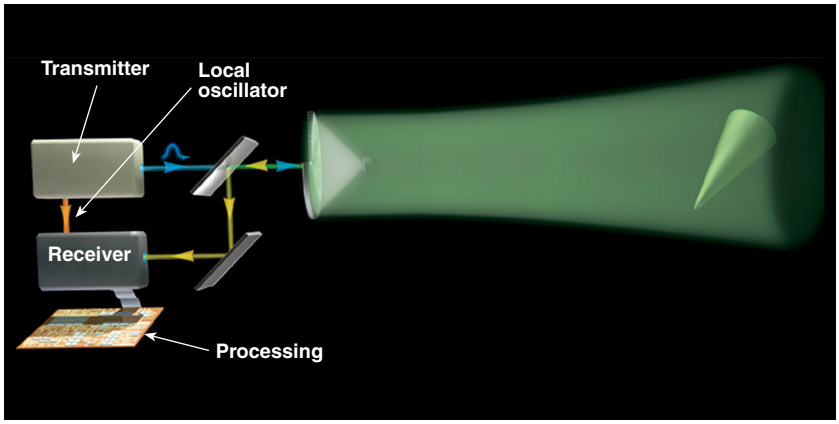

Figure 3. Main components of ladar systems.

electronic signal whose amplitude is proportional to the energy of the backscatter across time. Coherent detection is achieved by mixing the backscatter with a local oscillator beam generally derived from the laser source.

Measurement of range to target is accomplished by modulating the transmitted beam and observing the time of flight of the modulated pulse. Many modulation techniques developed for radar can also be implemented in ladar, including amplitude and frequency modulation. Incoherent ladar can measure range to target and the intensity of the received signal. The range resolution of ladar is limited by the bandwidth of the transmitted pulse. It is also possible to collect the received signal in consecutive range-resolution bins, producing the range profile along the line of sight, across the extent of the target.

The backscattered wavefront can be imaged in the ladar receiver on a focal plane array (FPA), where each pixel is a detector with range and/or intensity measurement capability. A FPA that measures range provides the angle-angle-range (AAR) image, a three-dimensional map of the illuminated target. Both the AAR image and the intensity image are diffraction-limited, and their angular resolution depends on wavelength and aperture size. Using a short wavelength such as 0.5 μm and an aperture diameter of 20 cm, the resolution on the target is 20 cm when the distance is 66 km. As illustrated in Fig. 1, AAR ladar has significantly better angular resolution than passive IR. In addition, AAR ladar provides range information that is not available with passive IR imaging. Typical wavelengths for AAR ladar are 1.06 μm obtained with Nd:YAG lasers and 0.50 μm obtained with frequency-doubled Nd:YAG lasers.

Coherent detection enables Doppler measurements whose resolution is limited by observation time and not by aperture size. In many cases the RV is spin-stabilized and the Doppler shifts due to axial rotation can be observed with the frequency measurement skill of coherent ladar. Furthermore, the spectral content in each range bin can be analyzed separately, giving rise to the range-Doppler signature of spinning objects. The effectiveness of this modality is limited by the signal-to-noise ratio (SNR) but not by diffraction. Therefore, informative range-Doppler signatures can be obtained at distances considerably larger than 200 km, and timely discrimination of the RV may be possible using features extracted from these signatures. The laser beam coherence required for these long distances is obtained, for example, with CO_2 lasers at 10.6 μm and Nd:YAG lasers at 1.06 μm.

This article presents an overview of the essential concepts involved in the formation of ladar data, the use of the data for discriminating the RV and guiding the interceptor missile, and related considerations that must be addressed for the study of ladar's potential. Range-Doppler ladar and discrimination of the spin-stabilized RV, range profiles, compensation of uncertainties in range and Doppler, and the three-dimensional images of AAR ladar are discussed.

RANGE DOPPLER

The relative motion of targets introduces a Doppler shift in the backscattered wavefront, and the received signal can be analyzed with spectral techniques to observe the Doppler information. In general, the target motion may have translational, rotational, and arbitrary components. The closing velocity between the ladar platform and the ballistic missile parts gives rise to the translational Doppler shift. The spectrum of the received signal can be used to determine this translational shift and to infer the closing velocity. An estimate of the closing velocity may contribute to the computation of target dynamics and trajectories. However, in the exo-atmosphere, most parts of the threat complex are likely to travel with similar speeds and trajectories, whose estimates have limited value for identifying the RV. The translational Doppler shift, which is several orders of magnitude larger than the other shift components, can be removed from the signal by using an adaptive local oscillator at the receiver. A feedback mechanism can adjust the local oscillator to a frequency close to the translational Doppler, enabling the heterodyne detector to produce a signal that contains only the Doppler shifts due to the slower motions of the objects. Removal of translational Doppler can also be accomplished with computational techniques.

After separation in the exo-atmosphere, in many cases the RV is spun to stabilize it in reentry and preserve the

established trajectory. This motion, which is intended to aim the ballistic missile, is also the source of an additional sensing dimension with good discrimination value. When the illuminated object is a spinning cone, the Doppler shift of surface points that turn toward the laser beam will increase the frequency, while the Doppler shift of those that turn away from the beam will decrease the frequency. Consequently, the entire object will impart a Doppler broadening that can be observed with appropriate frequency resolution and observation time. As with radar, Doppler broadening can be observed in each range bin by spectral analysis, producing the range-Doppler signature of the illuminated object. The aspect angle, defined between the laser beam orientation and the spin axis of the object, changes the range-Doppler signature significantly. Measured range-Doppler signatures of a spinning cone are shown in Figs. 4a and 4c. These signatures depend on geometric parameters of the object such as half cone angle, length, and aspect angle, as well as physical parameters such as wavelength, surface reflectance, and the angular velocity of the object. An analytical model that relates these parameters to the structure of range-Doppler signatures is essential for assessing the potential of range-Doppler ladar in discriminating the RV from other objects, including truncated cones (frustums) and cylinders that may also be spinning.

Range-Doppler Signature Model

An analytical model[4] of the range-Doppler signatures of rotating cones, frustums, and cylinders has been developed at APL and contributes to the study of observation requirements and discrimination algorithms. The model is developed by considering the object in the Cartesian coordinate system, rotating around its axis lying in the y–z plane, as in Fig. 5, which shows a cone of length h and base radius r_b. The incident collimated laser beam of wavelength λ is oriented along the z axis, and it is assumed to have a spot size large enough to contain the entire object. The surface material and the angle of incidence β between the optical axis and the surface normal $\mathbf{n}$ dictate the level of backscatter from any point. For a spinning cone, frustum, or cylinder, the Doppler shift Δf at each point is given by

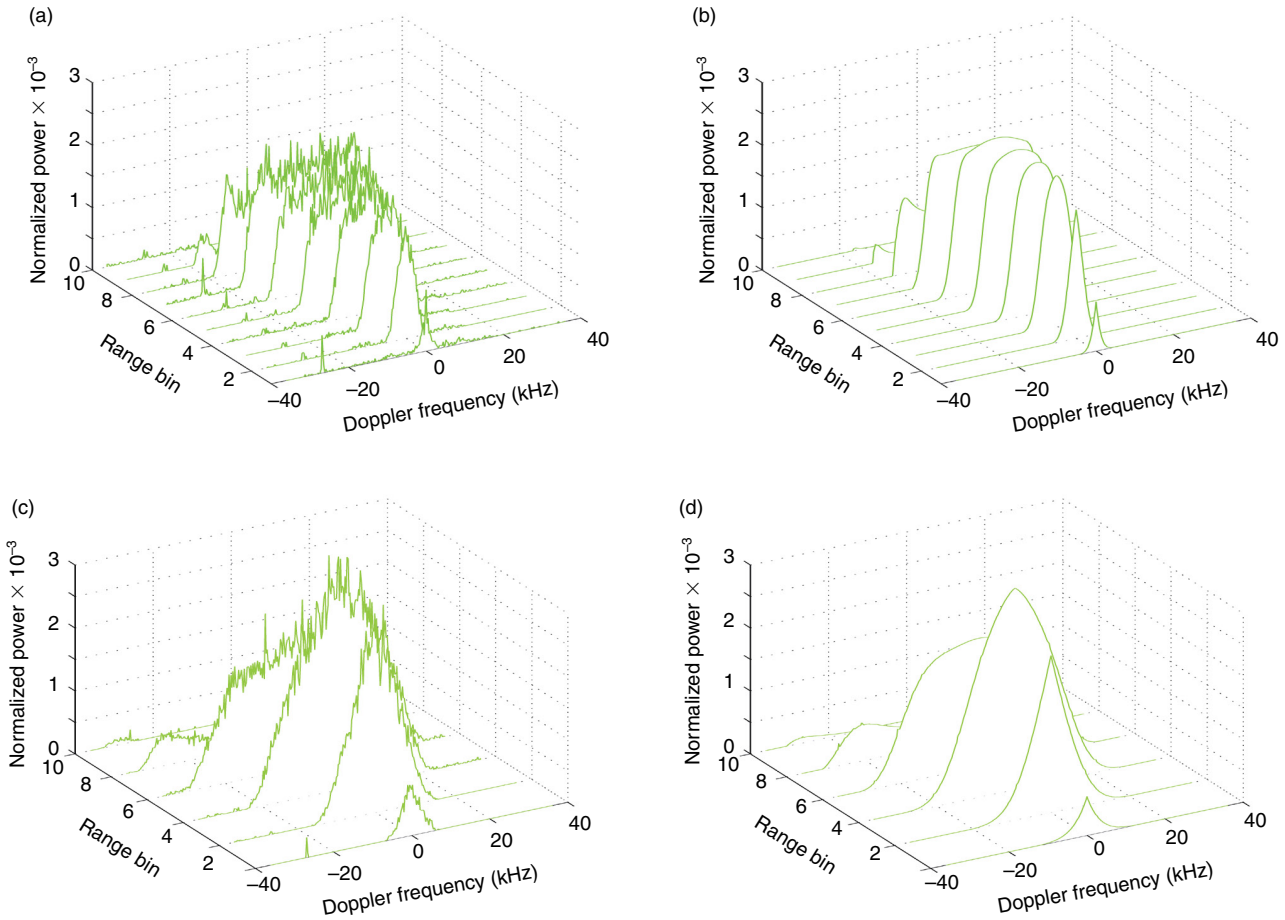

Figure 4. Experimental range-Doppler signatures of a spinning cone and corresponding model predictions: (a) data at 30° aspect angle, (b) model at 30° aspect angle, (c) data at 60° aspect angle, (d) model at 60° aspect angle.

$$\Delta f = \frac{2\omega r \cos\theta}{\lambda}, \tag{1}$$

where ω is the angular velocity, r is the radius at that point, and θ is the angle between the laser beam and the linear velocity vector $\mathbf{v}$ at that point. In the case of a cylinder, the magnitude of $\mathbf{v}$ is constant, but θ changes across the surface. The contribution of a small surface area element ΔA to the received power can be represented by

$$\Delta P(\beta) = K\rho(\beta)\Delta A \cos\beta, \tag{2}$$

where $\Delta P(\beta)$ is the incremental power contribution; K is a constant that depends on transmitted power, aperture size, propagation path length, transmittance, and beam divergence; and $\rho(\beta)$ is the backscatter reflectance that depends on the angle of incidence and the surface material. The magnitude of the power received in a given range bin depends on K, $\rho(\beta)$, and the area of the surface strip covered by the range bin, while the spectral distribution within a range bin is dictated by the Doppler shift of surface area elements. The two parameters r and θ, which establish the distribution of the Doppler shift across the object surface, are also related to the angle of incidence β. Using these relationships, Eq. 2 can be expressed as a function of Δf, leading to an analytical model of the Doppler spectrum in consecutive range bins.

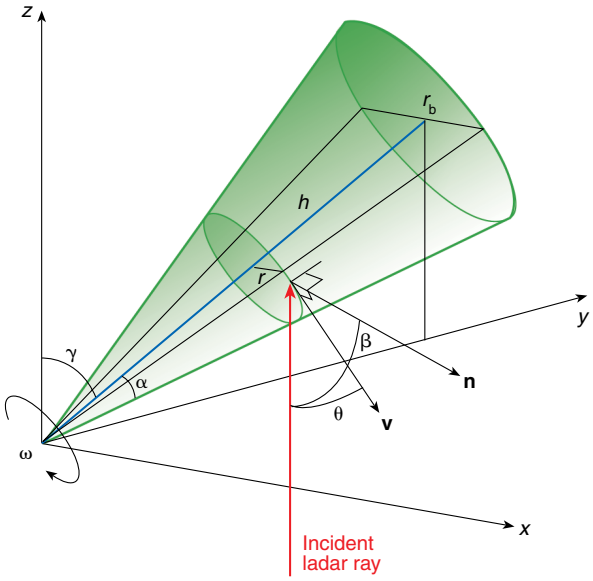

Figure 5. A cone in the model coordinate system. The ladar transmitter is assumed to be below the *x*–*y* plane, and parallel incident rays flood-illuminate the cone. One ray of the beam is shown. Each point on the illuminated section of the cone receives such a ray.

A conic or cylindrical surface whose axis is in the y–z plane can be represented by

$$\begin{aligned} f(x,y,z) = {} & x^2 + y^2(\cos^2\gamma - \tan^2\alpha \sin^2\gamma) \\ & + z^2(\sin^2\gamma - \tan^2\alpha \cos^2\gamma) \\ & - 2cy \tan\alpha \sin\gamma - 2cz \tan\alpha \cos\gamma \\ & - 2yz \sin\gamma \cos\gamma(1 + \tan^2\alpha) - c^2 = 0, \end{aligned} \tag{3}$$

where α is the half cone angle and γ is the aspect angle (Fig. 5). For a cylinder, c is the radius and $\alpha = 0$. For a cone, c dictates the position of the tip with respect to the origin, and for a frustum, c determines the location of the smaller base center. At any point on the surface, the z component of $\mathbf{n}$ (unit length) is equal to $\cos\beta$, and using the components of the surface gradient,

$$f_x = \frac{\partial f(x,y,z)}{\partial x}, \quad f_y = \frac{\partial f(x,y,z)}{\partial y}, \quad f_z = \frac{\partial f(x,y,z)}{\partial z}, \tag{4}$$

the angle of incidence can be obtained with

$$\cos\beta = \frac{f_z}{\sqrt{f_x^2 + f_y^2 + f_z^2}}. \tag{5}$$

The gradient components of the conic surface are

$$f_x = 2x, \tag{6}$$

$$f_y = \pm 2\sqrt{x^2(\tan^2\alpha \sin^2\gamma - \cos^2\gamma) + (z \tan\alpha + c\cos\gamma)^2}\ , \tag{7}$$

and

$$f_z = \frac{2z\tan^2\alpha + 2c\tan\alpha\cos\gamma \pm 2\sin\gamma\cos\gamma(1+\tan^2\alpha)\sqrt{x^2(\tan^2\alpha\sin^2\gamma - \cos^2\gamma) + (z\tan\alpha + c\cos\gamma)^2}}{\tan^2\alpha\sin^2\gamma - \cos^2\gamma}\ , \tag{8}$$

leading to

$$\cos\beta = -\frac{\sin\alpha\cos\alpha(z\sin\alpha + c\cos\alpha\cos\gamma) \pm \sin\gamma\cos\gamma\sqrt{x^2(\sin^2\alpha - \cos^2\gamma) + (z\sin\alpha + c\cos\alpha\cos\gamma)^2}}{\cos\alpha\cos\gamma(z\sin\alpha + c\cos\alpha\cos\gamma) \pm \sin\gamma\cos\alpha\sqrt{x^2(\sin^2\alpha - \cos^2\gamma) + (z\sin\alpha + c\cos\alpha\cos\gamma)^2}}. \tag{9}$$

The points illuminated by the laser beam are those for which $\cos\beta$ is negative, since these are points where the surface normal is oriented in the negative z direction, i.e., toward the ladar. Furthermore, the edge of the illuminated region on the surface is where the laser beam grazes the object with $\cos\beta = 0$.

To determine the relationship between β and Δf, it is possible to show that

$$r\cos\theta = \pm x\sin\gamma\ , \tag{10}$$

which, through Eq. 1, yields

$$x = \pm\frac{\lambda\Delta f}{2\omega\sin\gamma}\ , \tag{11}$$

and by substitution of Eq. 11 into Eq. 9, $\cos\beta$ can be expressed as a function of the physical parameters ω, λ, and Δf and the geometrical parameters α, c, γ, and z. The range-Doppler model must be a function of z and Δf (or Δx); therefore, the incremental surface area ΔA also must be expressed in terms of a grid in the coordinate system. Using a tessellation of the x–z plane with small increments Δx and Δz, we can state that

$$\Delta A = \frac{\Delta x\,\Delta z}{|\cos\eta|} = \Delta x\,\Delta z\left|\frac{\sqrt{f_x^2 + f_y^2 + f_z^2}}{f_y}\right|\ , \tag{12}$$

where η is the angle between the y axis and the surface normal at that point, and obtain

$$\Delta A = \Delta x\,\Delta z\, g(x,z), \tag{13}$$

with

$$g(x,z) = \left|\frac{\cos\alpha\cos\gamma(z\sin\alpha + c\cos\alpha\cos\gamma) \pm \sin\alpha\sin\gamma\sqrt{x^2(\sin^2\alpha - \cos^2\gamma) + (z\sin\alpha + c\cos\alpha\cos\gamma)^2}}{\cos\alpha(\sin^2\alpha - \cos^2\gamma)\sqrt{x^2(\sin^2\alpha - \cos^2\gamma) + (z\sin\alpha + c\cos\alpha\cos\gamma)^2}}\right|. \tag{14}$$

The reflectance of some materials may be diffuse Lambertian, typically modeled by

$$\rho(\beta) = k_L\cos\beta\ , \tag{15}$$

where k_L depends on the material; other materials may have a reflectance function that decays more rapidly with β such as

$$\rho(\beta) = k_E\exp(-\tau\beta), \tag{16}$$

where k_E and τ are the material constants. The reflectance of some materials can also be modeled as a linear combination of Eqs. 15 and 16.

Using Eqs. 2, 9, 11, and 13–16, the incremental power contribution can be expressed as a function of range and Doppler, with

$$\Delta P(z,\Delta f) = K\rho(z,\Delta f)\Delta x\,\Delta z g(z,\Delta f)\cos\beta(z,\Delta f)\,. \quad (17)$$

The spectrum of the received power that will be observed in a given range bin can be estimated by integrating the power over all points covered by that range bin and by taking into account the range-resolution function of the receiver. Range gating is the result of a convolution between the local pulse shape and the returning pulse as a function of time. Consequently, the range interval is defined by a window function $u(z)$ that is the outcome of this convolution and depends on the pulse shape of the laser. Laser pulses often have a shape close to a Gaussian,[5] and the range-resolution function $u_i(z)$ can also be approximated by a Gaussian,

$$u_i(z) = \frac{1}{\sigma\sqrt{2\pi}}\exp[-(z-z_i)^2/2\sigma^2]\,, \quad (18)$$

where z_i is the location of the center of the range interval i in the coordinate system of Fig. 5, and σ sets the range bin width. Therefore, the spectral content in the range bin i can be estimated with

$$P_i(\Delta f) = K\Delta x\int_{z_1}^{z_2} u_i(z)\rho(z,\Delta f)g(z,\Delta f)\cos\beta(z,\Delta f)dz\,, \quad (19)$$

where the limits z_1 and z_2 are $-\infty$ and $+\infty$ but can be set in practice to values such as $z_i - 3\sigma$ and $z_i + 3\sigma$.

This integration, however, should be carried out only on points that lie in the illuminated region and by taking into account the length of the object. Points in the illuminated region are those where $\cos\beta < 0$. If we set the origin to be at the tip of the cone ($c = 0$), and in the center of the lower base for the frustum or cylinder, the length h of the object introduces the constraint

$$0 < z < -y\tan\gamma + \frac{h}{\cos\gamma} \quad (20)$$

in the case of a cone and

$$-y\tan\gamma < z < -y\tan\gamma + \frac{h}{\cos\gamma} \quad (21)$$

in the case of the frustum and cylinder, both taken for $|\gamma| \le 90°$.

An initial validation of this model was performed using experimental ladar range-Doppler data from the Army Space and Missile Defense Command's Advanced Measurements Optical Range, a unique resource where ladar signatures of full-sized target objects are measured in an optically constructed far-field arrangement in a laboratory setting that obviates atmospheric effects during recordings. The range-Doppler signatures of a cone with $h = 1.5$ m, $\alpha = 12.7°$, and $\omega = 0.54$ rad/s, recorded with a 10.6-μm ladar, are shown in Fig. 4a for $\gamma = 30°$ and in Fig. 4c for $\gamma = 60°$. The corresponding model predictions are in Figs. 4b and 4d, respectively. Both experimental and modeled signatures are normalized to have a total power of unity. The goodness-of-fit, measured with the coefficient of determination, was 0.98 for $\gamma = 30°$ and 0.96 for $\gamma = 60°$.

In several APL programs, this model is used to simulate the signatures of spinning ballistic missile parts with varying shapes, sizes, materials, and spin rates as a function of aspect angle under adjustable noise levels. The effects of aspect angle, surface material, and object shape are illustrated in Fig. 6, where the range-Doppler signatures are simulated without noise to indicate the broad and fine structures of their fundamental spectral distributions. The level of detail that can be observed in a tactical setting will depend on the SNR of the range-Doppler signatures. Figure 7 illustrates simulated signatures at three SNR levels calculated as the mean of signal power to noise power ratio across all range-Doppler bins where a signal resides.

Discrimination with Range-Doppler Ladar

The potential of range-Doppler ladar depends on the information content of observed signatures, the effectiveness of discrimination features and algorithms, and the distances at which required discrimination levels can be accomplished. Three classes of objects have to be distinguished from the spin-stabilized RV: objects that do not spin, spinning objects that are not conic, and spinning cones that are not the RV (e.g., some decoys). These three classes, stated in order of increasing discrimination difficulty, require different algorithms of increasing complexity.

Objects that do not spin are characterized by a lack of Doppler broadening, and a good estimate of maximal Doppler extent can be used as the discriminating feature. Appropriate discrimination is achieved when the Doppler extent is observable, despite uncertainties introduced by noise and limited frequency resolution. Assuming conservative values for the spin rate and largest rotation radius, such as 2 rad/s (19.1 rpm) and 30 cm, respectively, the maximal linear velocity would be 60 cm/s. This gives rise to a maximal Doppler extent of 120 kHz with a 10-μm ladar and 1.2 MHz with a 1-μm ladar. A commensurate velocity resolution, for example 0.5 cm/s, requires frequency resolutions of 1 kHz at 10 μm and 10 kHz at 1 μm, obtained with observation

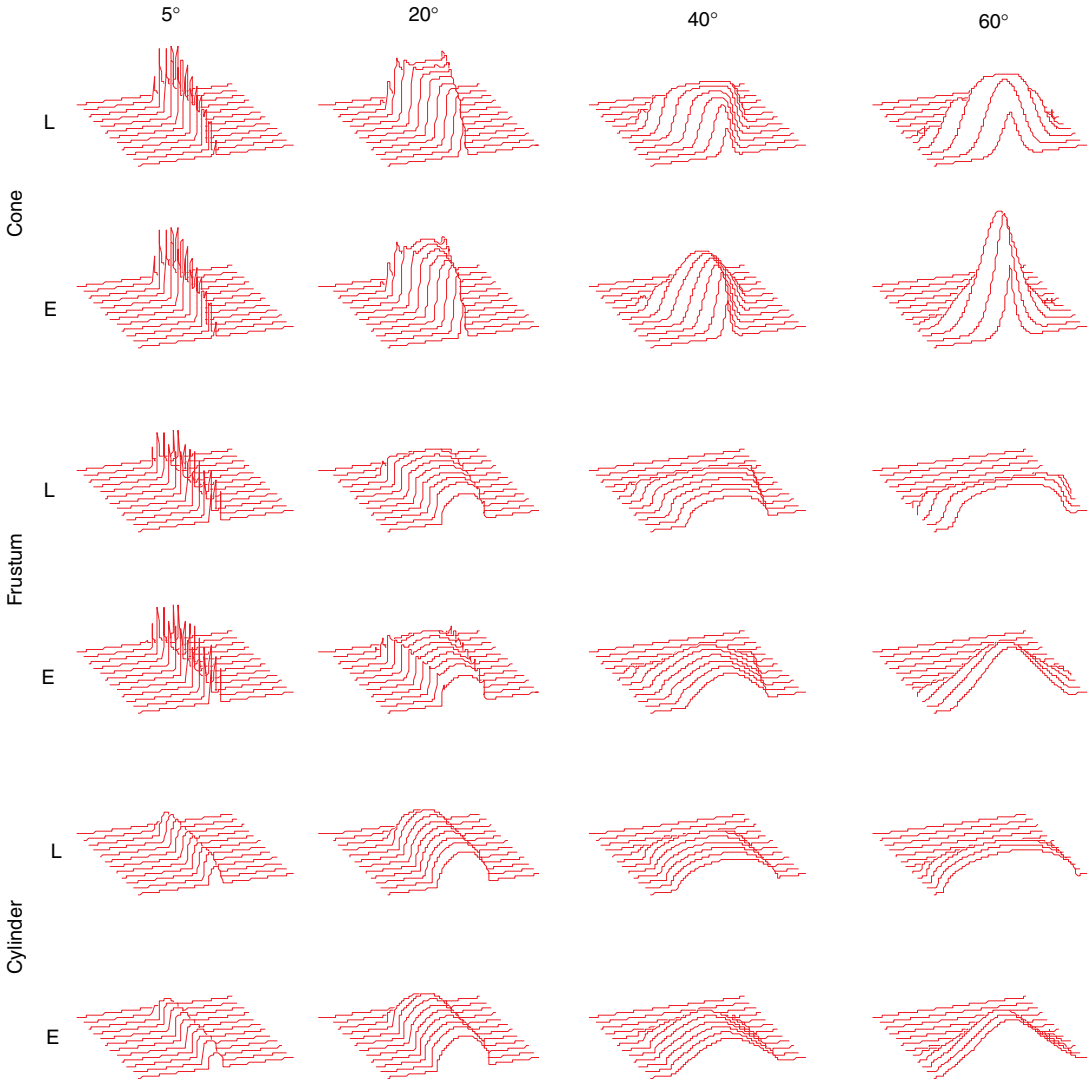

Figure 6. Simulated range-Doppler signatures of a cone, frustum, and cylinder with two surface materials (L = diffuse Lambertian, E = exponential reflectance) at four aspect angles. Each object is 2 m long and rotates with an angular velocity of 1 rad/s. Each signature consists of 12 range bins, plotted in a Doppler interval of –80 to +80 kHz.

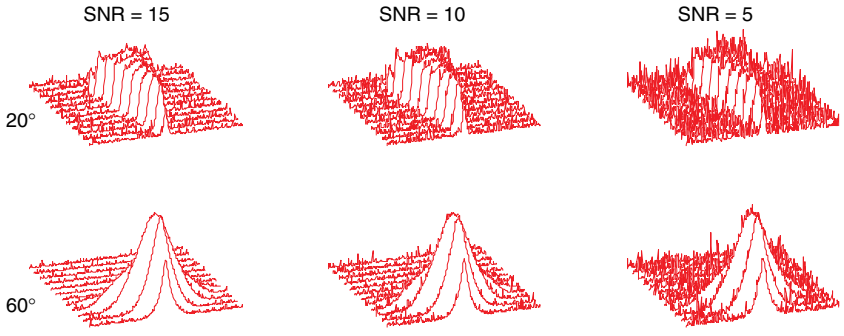

Figure 7. Range-Doppler signatures of a 2-m-long cone with exponential reflectance, rotating at 1 rad/s at two aspect angles and simulated at three SNR levels. Each signature has 12 range bins, and their spectral content is shown in the Doppler interval of –80 to +80 kHz.

times of 1.0 and 0.1 ms, respectively. Using these frequency resolutions, and when aspect angles are wider than about 2°, 99% correct discrimination requires the SNR to be 8 for algorithms based on simple thresholding, while more elaborate algorithms can achieve the same level of discrimination with significantly lower SNR levels. Studies suggest that the required SNR levels can be obtained at distances in excess of 300 km from the objects. When the aspect angle is very small, spinning objects do not introduce significant Doppler broadening because all points spin in a plane approximately perpendicular to the laser beam. The limiting aspect angle depends on the spin rate of the object.

Spinning objects that are not conic require a discrimination algorithm that can distinguish signatures such as those in the four bottom rows of Fig. 6 from those in the two top rows. Here, discriminating features can be obtained from the spectral edge line across range bins. The spectral edges of a range bin are two homologous frequency points where the spectrum is down to a low value (e.g., noise level) on either side of the zero-Doppler point. The absolute value of the two spectral edges can be averaged to reduce the effects of noise, leading to one value per range bin. In the range-Doppler plane, a line that passes from the spectral edge points in consecutive range bins has different properties for the three types of objects, as shown in Fig. 8, where the dependence on spin rates and aspect angles is also illustrated. Evidently, the vertical axis intercept of these lines has good discrimination value, and other features such as the slope of the line and number of range bins can contribute to discrimination. Using these features, the spinning RV can also be discriminated from the other spinning shapes at distances of 300 km or more, depending on the power-aperture product of the ladar.

The most challenging discrimination task is separation of the spinning RV from spinning decoys that have the same size, shape, and surface material as the RV. Although in some cases the spin rates of the RV and decoy may differ, spin rate is not a good discriminant because the associated observable, Doppler broadening, does not depend on the spin rate alone. In a given range

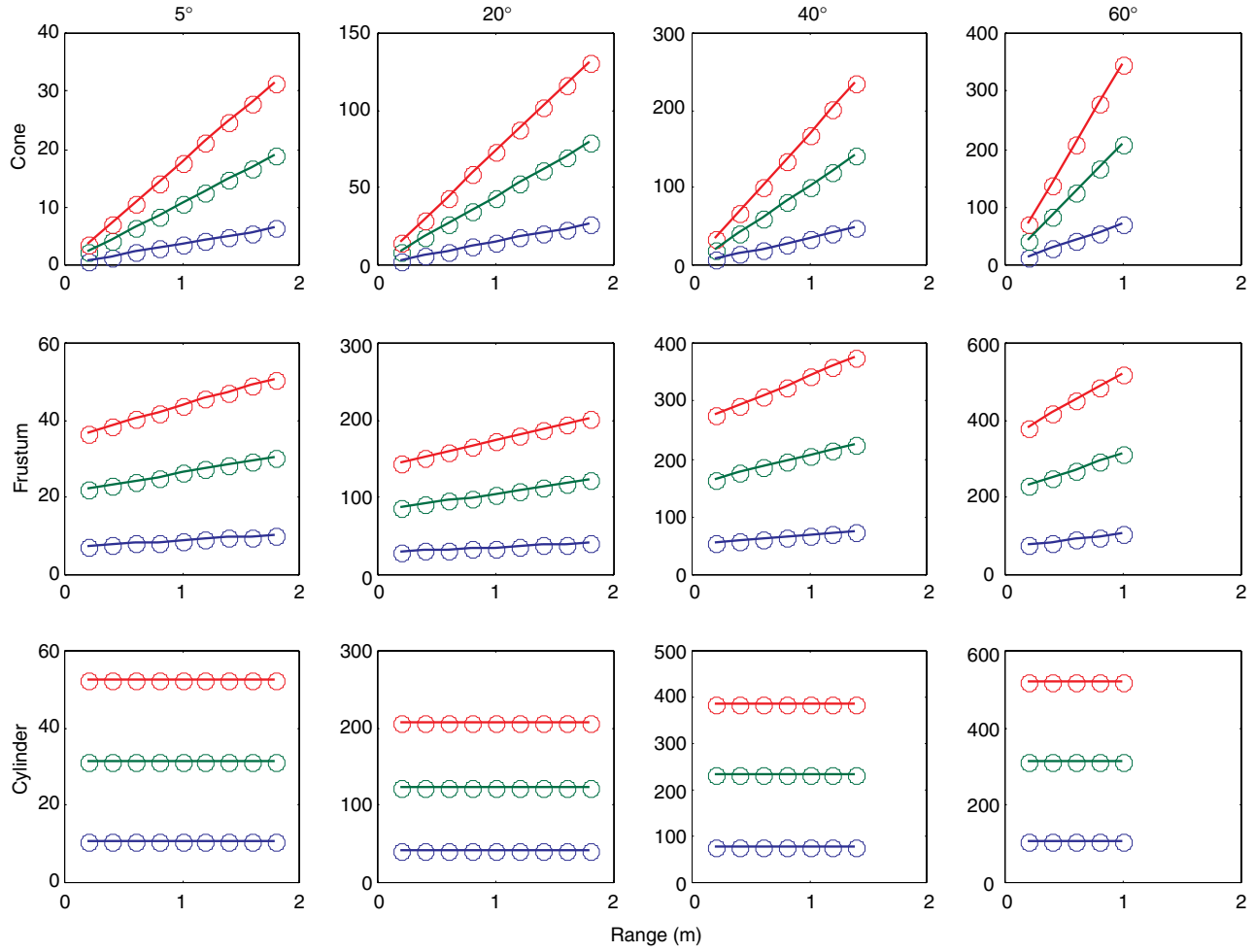

Figure 8. Spectral edge lines in range-Doppler signatures of the three object types at four aspect angles. In each panel, the spin rates are 1, 3, and 5 rad/s for blue, green, and red curves, respectively.

bin, the one-sided Doppler extent f_r on one side of the zero-Doppler point is

$$f_r = \frac{2\omega r \sin\gamma}{\lambda}, \tag{22}$$

where r is the largest radius contained in that bin. Therefore, two cones spinning at different rates can exhibit similar Doppler broadening if their aspect angles allow.

Spinning cones also have a precession motion about their center of gravity which is characterized by its own rate and angle. During precession, the aspect angle changes with time t acccording to

$$\gamma(t) = \cos^{-1}(\sin\delta \sin\gamma_0 \sin\omega_p t + \cos\delta \cos\gamma_0), \tag{23}$$

where δ is the precession angle, γ_0 is the mean aspect angle, and ω_p is the precession rate. The precession rate or the precession angle can be used as a discriminating feature to distinguish the RV from decoys if these two types of objects have significantly different precession rates or precession angles. The precession rate is typically an order of magnitude slower than the spin rate ω, and the precession angle is also relatively small compared to the half cone angle α. Therefore, the Doppler shift component due to precession may be difficult to observe. However, precession manifests itself as a periodic change in aspect angle. Consequently, since the spin rate can be considered constant during engagement, the precession rate can be estimated by observing f_r in Eq. 22 as it changes with γ. A Doppler extent measurement can be made on each range bin, but the bin with the highest radius provides the largest Doppler extent with the highest modulation.

The accuracy of the measurement of changes in f_r is dictated by the amount of modulation due to changing aspect angle, the frequency resolution, and the SNR. The accuracy of f_r, along with the temporal resolution across a precession period, determines the accuracy of the estimation of the precession period. A 10-μm ladar with a coherent observation time of 1 ms, collecting several signatures every second, can provide a precession rate estimate with less than a 2% error when precession angles are higher than 1° and spin rates are faster than 1 rad/s at moderate SNR levels. It may be possible to measure relatively small differences in precession rates.

If the decoy is matched also by precession rate, it may have a different precession angle than that of the RV. An estimate of the precession angle may be obtained only if the aspect angle can be estimated as a function of time. Aspect angle estimation is one of the most demanding measurements and requires a series of range-Doppler signatures of the same object taken at sufficiently different aspect angles each time. An APL-developed algorithm uses the slope and frequency extent information of the spectral edge lines and solves an overdetermined system to give an estimate of aspect angle γ_i for each signature in the series. The average of aspect angles taken over a precession period is a good estimate of the mean aspect angle γ_0, and the precession angle δ can be inferred from Eq. 23 since the set γ_i is a discrete representation of $\gamma(t)$.

RANGE PROFILE

If the RV is not spin-stabilized, it will tumble at rates relatively slower than the spin rates. Because of the slow rates and the potentially irregular motion of tumbling, Doppler information may not be as informative as the spin-stabilized case. Then, the range binning function of ladar can be used to obtain range profiles of the RV and other objects. Figure 9 shows the simulated range

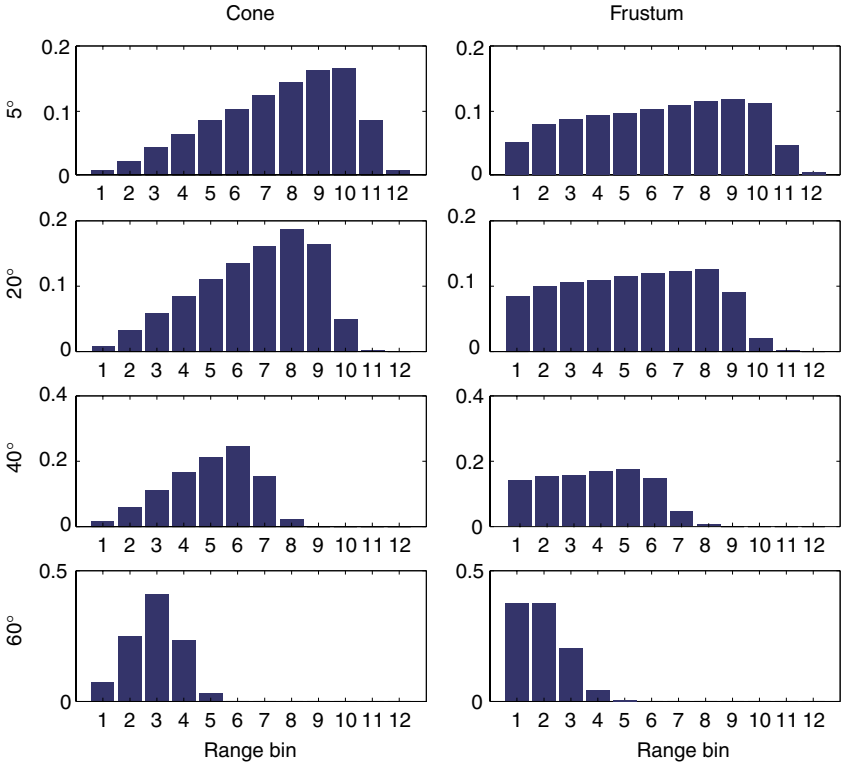

Figure 9. Simulated range profiles of the cone and frustum in Fig. 6 (exponential reflectance) at four aspect angles.

profiles of a cone and frustum at four different aspect angles, with a range resolution of 20 cm. Using these signatures, feature extraction and pattern recognition algorithms distinguish cones from frustums at reasonable SNR levels. Discrimination of cones from cylinders is also possible using range profiles. Discrimination of the RV from a conic decoy may be possible if there are significant differences between the tumbling dynamics of the RV and those of the decoy. For example, the dominant tumbling rate can be estimated by observing the modulation of the range profile across time. The accuracy of such estimates depends on the range resolution, temporal sampling rate, and SNR.

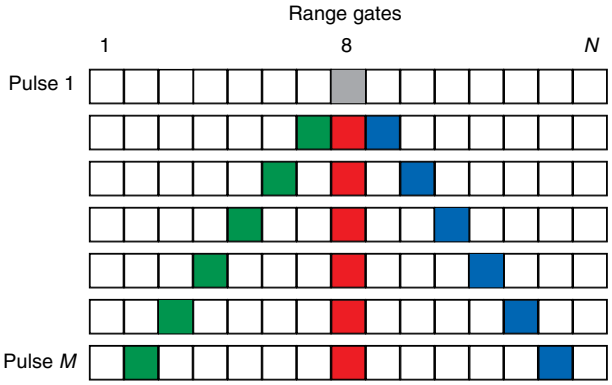

Figure 10. Range walk compensation search strings across *M* pulses, each with *N* range bins.

RANGE WALK AND DOPPLER WALK COMPENSATION

When a range profile or range-Doppler observation starts, although some prior information may be available, a considerable uncertainty in range, rate of change in range (range rate), and Doppler will be present. Furthermore, since closing speeds are particularly high, the range will decrease rapidly and the Doppler amount may also change owing to the trajectories of interceptor and target. Consequently, the ladar receiver must perform a limited search in range, range rate, and Doppler to lock on the target returns and track them accordingly. The quality of range profile and range-Doppler signatures depends on the effectiveness of range walk and Doppler walk compensation algorithms.

Depending on the wavelength, a coherent ladar observation for ballistic missile targets may need to be about 1 ms long, during which the distance to target can become a few meters shorter. Considering 20-cm range gates, during a coherent observation, the target may walk across more than 20 range gates in the absence of compensation. Available prior information on range rate may provide some initial compensation, and by sliding range gates accordingly, range walk can be reduced, for example, to six gates during coherent observation. The process typically results in some residual range walk toward or away from the seeker. To determine and maintain the best possible compensation, the ladar receiver search in range and range rate is organized such that each range-gate hypothesis is implemented by considering several range-rate possibilities that span the entire range-rate uncertainty. Each range-rate hypothesis assumes that the uncompensated range walk occurs at a distinct rate in a given direction.

Figure 10 illustrates the search process across a coherent observation of *M* pulses, each analyzed with *N* range gates. The figure shows the range gates aligned after the initial compensation, such that if there were no uncompensated walk, each range gate would correspond to the homologous one in every pulse. For each range gate of the first pulse, a search with multiple strings is performed across all pulses. Only the search for range gate 8 is illustrated in Fig. 10. In the absence of residual walk, the correct string would be the vertical (red) one, and returns from gate 8 in each pulse would represent the return from the same slice of the target. Other range-rate hypotheses lead to other strings on either side of the central one. The blue string in Fig. 10 corresponds to a hypothesis that produces a walk of six gates across the coherent observation interval. Assuming that this string and the symmetrical green string span the range-rate uncertainty, a number of such strings between the two extremes can be tested to determine the best hypothesis. The number of strings is generally selected to provide an error equal to a fraction of a range gate between the actual walk and the best hypothesis across all M pulses. This ensures a reasonable SNR loss in the range walk compensator. The best hypothesis is the one that results in the highest SNR after coherent processing.

Aside from maintaining the integrity of the range gates across all pulses, it is necessary to ensure that the Doppler observation is not impaired by range-rate error. This requires that the coherent filtering operations, which generally include a fast Fourier transform (FFT), unambiguously span the Doppler uncertainty while minimizing SNR losses. In addition to range-rate error, Doppler observations may be degraded by acceleration along the line of sight because the accelerated return has a time-varying Doppler across the coherent interval. If the smear in Doppler is a fraction of the FFT resolution, the loss due to unaccounted acceleration can be tolerated; otherwise, Doppler walk compensation must be implemented. Doppler walk compensation functions similarly to range walk compensation, performing a frequency-rate search with multiple strings for each FFT resolution cell. The search should span the uncertainty in acceleration such that Doppler smear is kept to a fraction of the FFT resolution. Doppler walk compensation is imparted by shifting the phase of the complex FFT coefficients by an amount that accounts for the acceleration uncertainty.

ANGLE-ANGLE-RANGE

Generally the intensity profile across laser beams used in ladar is Gaussian, and the corresponding beam divergence is given by

$$w(z) = w_0 \sqrt{1 + \left(\frac{\lambda z}{\pi w_0^2} \right)^2}, \qquad (24)$$

where $w(z)$ is the beam radius at a distance z, and w_0 is the beam waist, which will be assumed to occur at the telescope transmit aperture whose diameter $d_t = 2w_0$. The illuminated area has a diameter of twice $w(z)$ at a distance z from the telescope, and we will consider the case where the entire illuminated area is mapped on the FPA of the receiver. Considering an $n \times n$ FPA, each pixel will be mapped, at the distance z, onto a section of size $s = 2w(z)/n$. The physical diffraction limit imposes a minimal spatial resolution given by

$$s_d = \frac{1.22\lambda}{d} z, \qquad (25)$$

where d is the receive aperture diameter, which may be bigger than d_t if so designed. To avoid blur due to diffraction, $s_d \leq s$ must be ensured with an appropriate choice of d. Using the generalized cone formulation in Eq. 3 and boundary conditions from Eqs. 9 and 20, we can model the AAR images that will be obtained with specified choices of λ, d, and n as a function of the aspect angle γ. Figure 11 shows simulated AAR images of an RV at four aspect angles observed from 33 km with a wavelength of 0.5 μm, a receive aperture d = 20 cm, and a 32×32 FPA. In this case, the cross-range resolution on the target is 10 cm.

For effective impact, the interceptor missile should be guided to an aimpoint that is preferably on the axis of the cone, a certain distance away from the tip. The location of this desired region on the target can be determined using the three-dimensional information of AAR images such as orientation, length, and location of tip. For most aspect angles, good estimates of these parameters can be obtained when the resolution is as good as in Fig. 11. AAR ladar at 0.5 μm provides this resolution from 33 km, 8 times farther than the distance needed by passive IR for the same resolution, using the same aperture size.

DISCUSSION

Short wavelengths of ladar provide high resolution in angle and Doppler, leading to range-Doppler, range-profile, and AAR signatures that can convey information on the shape and dynamics of ballistic missile objects. The value of ladar in Ballistic Missile Defense will ultimately be determined by the technologically and tactically feasible implementations of the techniques described here.

Any sensor used for discrimination will be effective only if its observations and inferred parameters have enough information to distinguish the RV from all other objects in the threat complex. If the threat complex includes decoys whose shape, material, and dynamics are similar to those of the RV, decoys cannot be distinguished from the RV using any sensor. Therefore, discrimination with ladar is based on the assumption that there will be observable differences in the shape, size, orientation, rotation, precession, or tumbling of the RV compared to all other objects. Differences in thermal properties cannot be sensed with ladar. Since ladar must be cued by another sensor, it is very likely that ladar

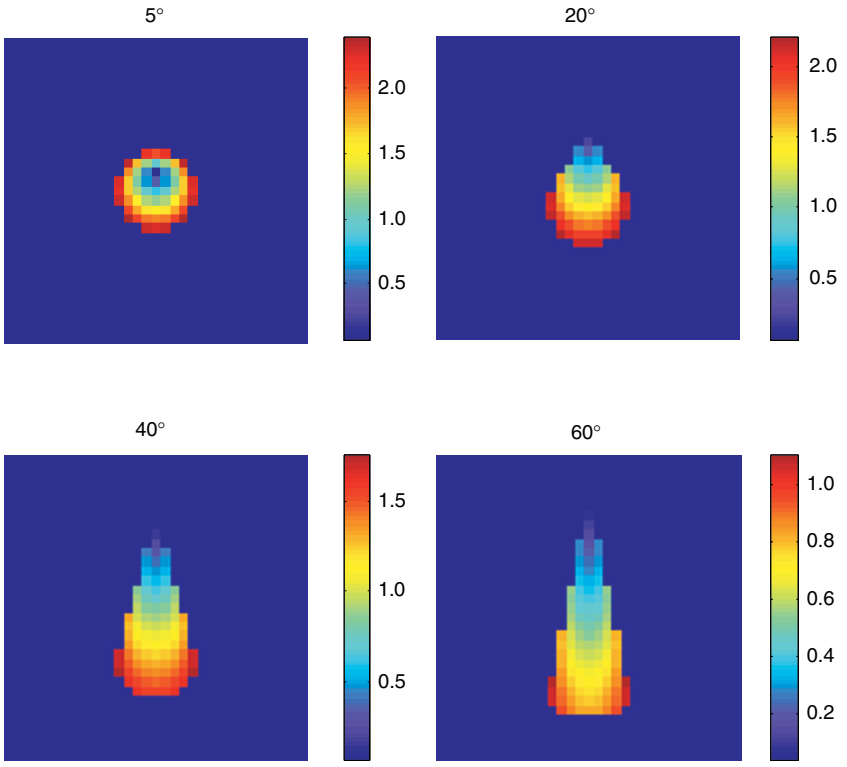

Figure 11. Simulated three-dimensional AAR ladar images of an RV at various aspect angles observed with a spatial resolution of 0.1 m on the object. The tip of the cone is oriented toward the ladar. The depth dimension is shown with the color map, ranging from 0 at the tip to more than 2 m in small aspect angles.

and passive IR will operate jointly and the latter will be available to exploit thermal information.

Discrimination of the spinning RV can best be accomplished by range-Doppler ladar since the Doppler dimension is particularly valuable in this case. Discrimination performance depends on range and frequency resolutions, the SNR of the signatures, and aspect angle. At long distances, each object in the threat cluster will be mapped onto one pixel of the AAR ladar. On such images, the precession of the RV manifests itself as a modulation in range, which may also be used for discrimination. Passive IR has potential for discriminating the spinning RV since the precession causes intensity modulation in the IR pixel. Discrimination of the RV that is not spin-stabilized can be addressed with range-profile ladar, AAR ladar, and passive IR. Tumbling will cause range modulation in range-profile and AAR ladars and intensity modulation in passive IR. The comparative merits of ladar and passive IR for discrimination of the tumbling RV remain to be determined.

At distances shorter than 20 km, both passive IR and AAR ladar have angular resolution for aimpoint selection. However, at the same distance, AAR ladar can provide significantly higher resolution than passive IR. Owing to higher angular resolution and three-dimensional information, AAR ladar may lead to higher aiming accuracy in guiding the interceptor to the impact point.

To ensure the best SNR, the most appropriate platform for ladar seems to be the interceptor. Onboard the interceptor, however, both the transmitter and receiver will be subject to vibrations whose amplitude and spectral content will vary with the missile design. Vibrations may affect laser beam pointing, imaging performance, and the alignment of the heterodyne detector in coherent ladar. Although most of the appreciable vibration amplitudes occur in the low-frequency regime, in some cases the small amplitudes that may be present at higher frequencies may also affect the interferometric process of the Doppler observations. Stabilization and compensation techniques will play a particularly important role for ladar on an interceptor.

Compared to radar and passive IR, the technology of ladar is less mature, and systems that can be integrated in seekers are currently under development. The effectiveness of ladar in Ballistic Missile Defense will have to be determined with analytical studies, simulations, hardware testing and evaluation, field tests, and interception tests.

REFERENCES

[1] Kamerman, G. W., "Laser Radar," in *Active Electro-Optical Systems, The Infrared and Electro-Optical Systems Handbook*, Vol. 6, C. S. Fox (ed.) (1993).
[2] Jelalian, A. V., *Laser Radar Systems*, Artech House, Boston, MA (1992).
[3] Bachman, C. G., *Laser Radar Systems and Techniques*, Artech House, Dedham, MA (1979).
[4] Bankman, I. N., "Analytical Model of Doppler Spectra of Coherent Light Backscattered from Rotating Cones and Cylinders," *J. Opt. Soc. Am. A* **17**, 465–476 (2000).
[5] Siegman, A. E., *Lasers*, University Science Books, Sausalito, CA (1986).

THE AUTHORS

ISAAC N. BANKMAN, a member of the APL Principal Professional Staff, is Supervisor of the Imaging and Laser Systems Section in ADSD's Electro-Optical Systems Group. He received a B.S. in electrical engineering from Bosphorus University, Turkey, in 1977, an M.S. in electronics from the University of Wales, Britain, in 1979, and a Ph.D. in biomedical engineering from Technion University, Israel, in 1985. He joined APL in 1990 and worked on signal processing algorithms for transient detection, image processing algorithms for object recognition, and image registration algorithms. In the past 6 years he has developed analytical models of ladar and radar signatures of ballistic missile parts and related discrimination algorithms. His recent work also includes ladar sensing and laser communication in marine applications, image analysis for missile guidance, and radar and passive IR fire control systems for ship self-defense. His e-mail address is isaac.bankman@jhuapl.edu.

ERIC W. ROGALA, a member of APL's Senior Professional Staff, is with the Electro-Optical Systems Group in ADSD. He received B.S. and M.S. degrees in optical sciences from the University of Rochester in 1990 and 1992, respectively. In 1999 he received a Ph.D. in optical engineering from the University of Arizona's Optical Sciences Center for his theoretical and experimental work on a novel phase-shifting interferometer capable of mapping the profile and complex index of refraction of a surface. In March 2000 Dr. Rogala joined ADSD's Electro-Optical Systems Group and has been involved in designing and analyzing optical systems as well as developing pattern recognition software. His current interests include automated target recognition in passive IR imagery, automated analysis of solar flare images, boresight error analysis in sapphire dome for SM-2 Block IVA, modeling of 3-D laser radar images, and phase-shifting interferometry of biological cells. His e-mail address is eric.rogala@jhuapl.edu.

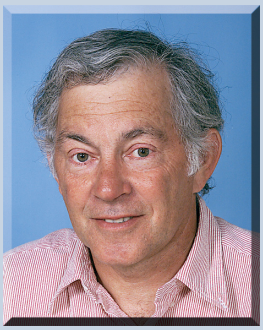

RICHARD E. PAVEK, a member of the APL Principal Professional Staff, is with the Combat Systems Development Group of ADSD, where he conducts radar system conceptual designs and analyses and manages research tasks. He has B.S. and M.S. degrees in electrical engineering from the University of Illinois and an Engineer degree in electrical engineering from USC. He joined APL in 1991 after a 20-year career at Hughes Aircraft, where he was involved in the development of the active and semi-active radar in the Navy's Phoenix and AMRAAM missiles. He designed low-altitude techniques that use diffuse multipath in airborne and ship radars to better overcome ECM and multipath limitations, and developed multisensor, countermeasure, and target association techniques for CEC. His current work focuses on the ballistic missile discrimination problem, random waveforms, and various advanced super-resolution and SAR schemes for diverse platforms. His e-mail address is richard.pavek@jhuapl.edu.